Nano-Hexapod - Test Bench

Dehaeze Thomas

October 27, 2024

Contents

In the previous section, all the struts were mounted and individually characterized. Now the nano-hexapod is assembled using a mounting procedure described in Section 1.

In order to identify the dynamics of the nano-hexapod, a special suspended table is developed which consists of a stiff "optical breadboard" suspended on top of four soft springs. The Nano-Hexapod is then fixed on top of the suspended table, such that its dynamics is not affected by complex dynamics except from the suspension modes of the table that can be well characterized and modelled (Section 2).

The obtained nano-hexapod dynamics is analyzed in Section 3, and compared with the Simscape model in Section 4.

1 Nano-Hexapod Assembly Procedure

The assembly of the nano-hexapod is quite critical to both avoid additional stress in the flexible joints (that would result in a loss of stroke) and for the precise determination of the Jacobian matrix. The goal is to fix the six struts to the two nano-hexapod plates (shown in Figure 1.1a) while the two plates are parallel, aligned vertically, and such that all the flexible joints do not experience any stress. Do to so, a precisely machined mounting tool (Figure 1.1b) is used to position the two nano-hexapod plates during the assembly procedure.
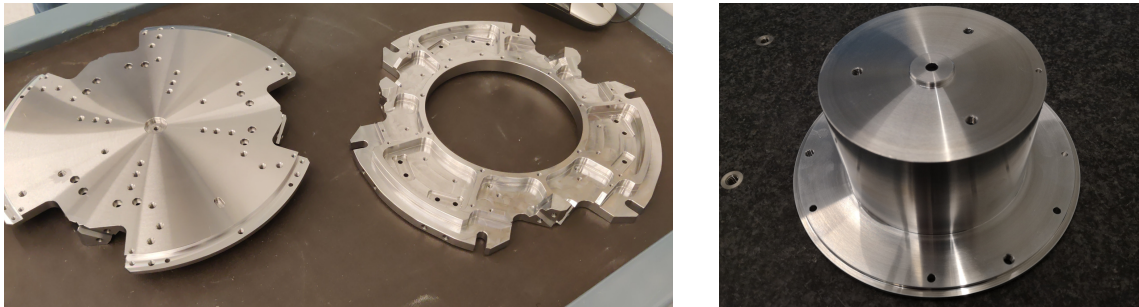
(a) Received top and bottom plates

(b) Mounting tool

Figure 1.1: Received Nano-Hexapod plates (a) and mounting tool used to position the two plates during assembly (b)

The mechanical tolerances of the received plates are checked using a FARO arm[1] (Figure 1.2a) and are found to comply with the requirements[2]. The same is done for the mounting tool[3] The two plates are then fixed to the mounting tool as shown in Figure 1.2b. The main goal of this "mounting tool" is to position the flexible joint interfaces (the "V" shapes) of both plates such that a cylinder can rest on the 4 flat interfaces at the same time.

The quality of the positioning can be estimated by measuring the "straightness" of the top and bottom "V" interfaces. This corresponds to the diameter of the smallest cylinder that contains all points of the measured axis. This is again done using the FARO arm, and the results for all the six struts are summarized in Table 1.1. The straightness is found to be better than $15\,\mu m$ for all the struts[4], which is sufficiently good to not induce significant stress of the flexible joint during the assembly.

The encoder rulers and heads are then fixed to the top and bottom plates respectively (Figure 1.3). The encoder heads are then aligned to maximize the received contrast.

The six struts are then fixed to the bottom and top plates one by one. First the top flexible joint is

---

[1]Faro Arm Platinum 4ft, specified accuracy of $\pm 13 \mu m$

[2]Location of all the interface surfaces with the flexible joints are checked. The fits (182H7 and 24H8) with the interface element are checked.

[3]The height dimension is better than $40\,\mu m$. The diameter fit of 182g6 and 24g6 with the two plates is verified.

[4]As the accuracy of the FARO arm is $\pm 13\,\mu m$, the true straightness is probably better than the values indicated. The limitation of the instrument is here reached.
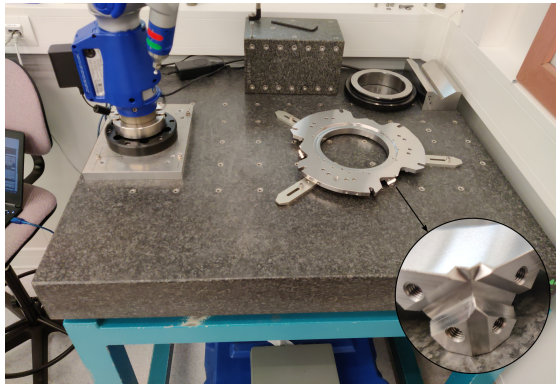
(a) Dimensional check of the bottom plate
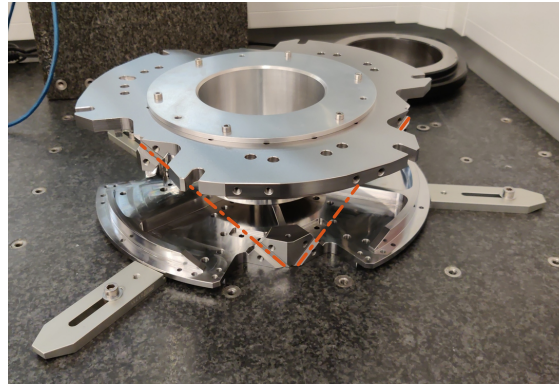
(b) Wanted coaxiality between interfaces

Figure 1.2: A Faro arm is used to dimensionally check the received parts (a) and after mounting the two plates with the mounting part (b)

Strut	Meas 1	Meas 2
1	$7\,\mu m$	$3\,\mu m$
2	$11\,\mu m$	$11\,\mu m$
3	$15\,\mu m$	$14\,\mu m$
4	$6\,\mu m$	$6\,\mu m$
5	$7\,\mu m$	$5\,\mu m$
6	$6\,\mu m$	$7\,\mu m$

Table 1.1: Measured straightness between the two "V" for the six struts. These measurements are performed two times for each strut.

(a) Encoder rulers
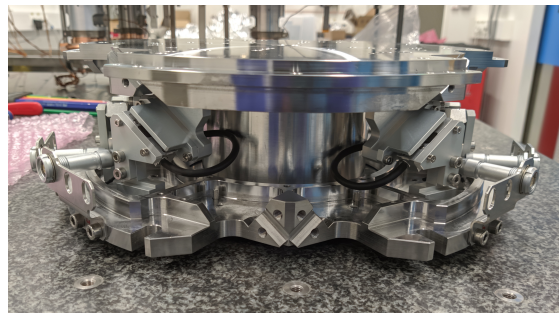
(b) Encoder heads

Figure 1.3: Mounting of the encoders to the Nano-hexapod. The rulers are fixed to the top plate (a) while the encoders heads are fixed to the botom plate (b)

fixed such that its flat reference surface is in contact with the top plate. This is to precisely known the position of the flexible joint with respect to the top plate. Then the bottom flexible joint is fixed. After all six struts are mounted, the mounting tool (Figure 1.1b) can be disassembled, and the fully mounted nano-hexapod as shown in Figure 1.4 is obtained.
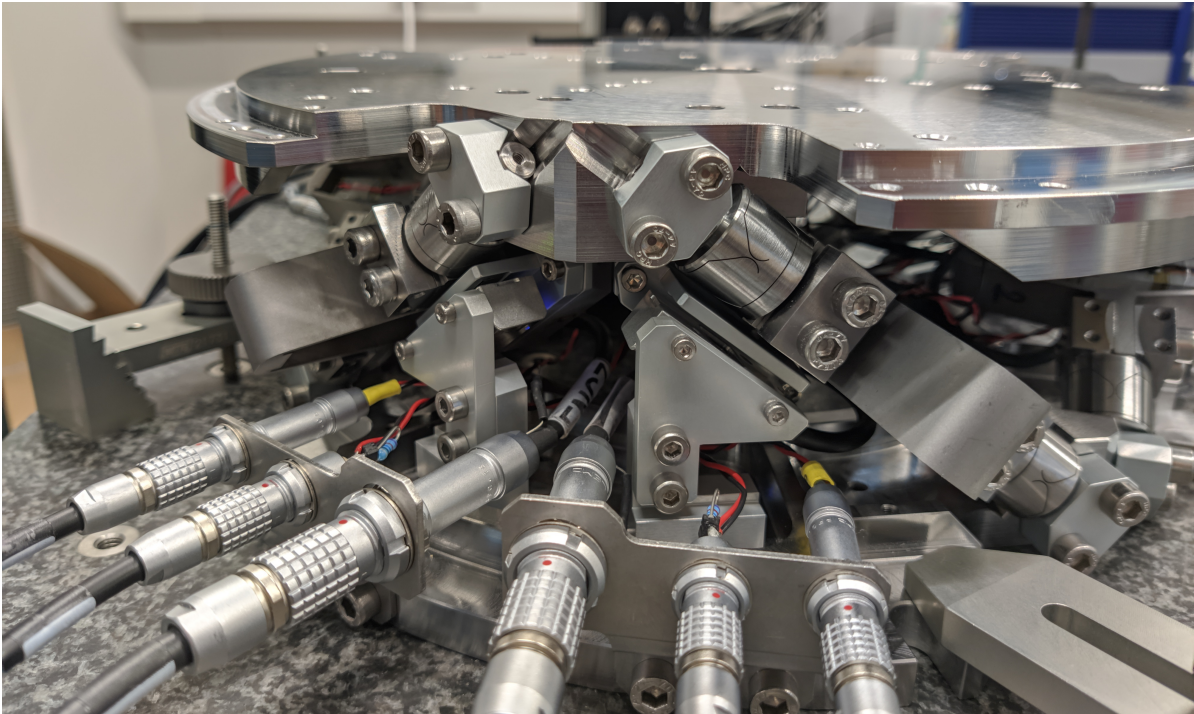

Figure 1.4: Mounted Nano-Hexapod

2 Suspended Table

2.1 Introduction

This document is divided as follows:

- Section 2.2: the experimental setup and all the instrumentation are described

- Section 2.3: the table dynamics is identified

- Section 2.4: a Simscape model of the vibration table is developed and tuned from the measurements

2.2 Experimental Setup

Redo the CAD view

2.2.1 Suspended table

Dimensions 450 mm x 450 mm x 60 mm

Mass 21.3 kg (bot=7.8, top=7.6, mid=5.9kg)

Interface plate 3.2kg

If we include including the bottom interface plate:

- Total mass: 24.5 kg

- CoM: 42mm below Center of optical table

- Ix = 0.54, Iy = 0.54, Iz = 1.07 (with respect to CoM)

2.2.2 Springs

Helical compression spring make of steel wire (52SiCrNi5) with rectangular cross section SZ8005 20 x 044 from Steinel L0 = 44mm Spring rate = 17.8 N/mm

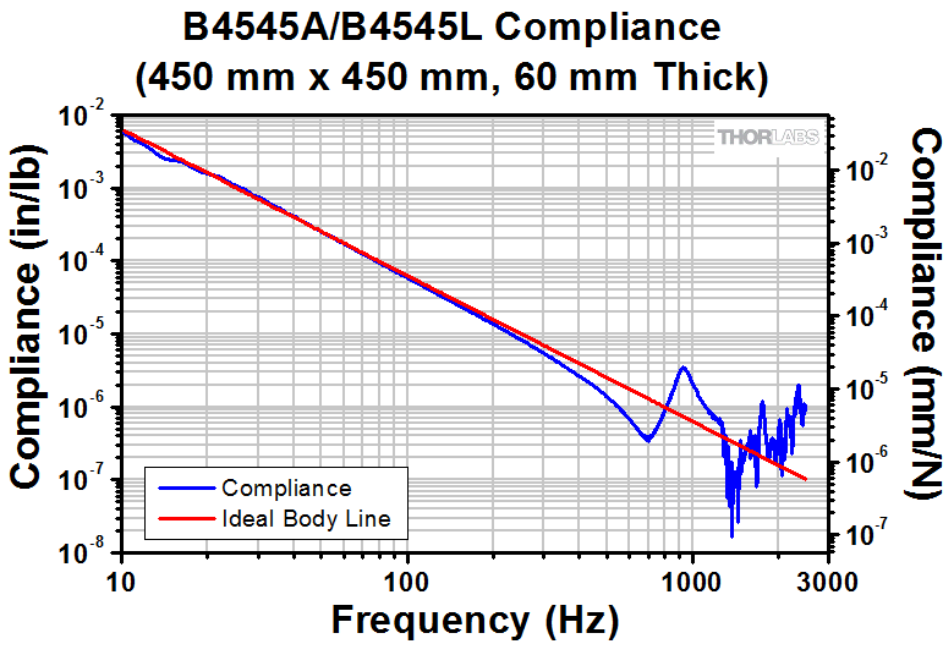**Figure 2.1:** CAD View of the vibration table

Figure 2.2: Compliance of the B4545A optical table

2.3 Identification of the table's response

(4x) 3D accelerometer PCB 356B18

	Freq. [Hz]	Description
1	1.3	X-translation
2	1.3	Y-translation
3	1.95	Z-rotation
4	6.85	Z-translation
5	8.9	Tilt
6	8.9	Tilt
7	700	Flexible Mode

Table 2.1: List of the identified modes

2.4 Simscape Model of the suspended table

In this section, the Simscape model of the vibration table is described.

2.4.1 Simscape Sub-systems

Parameters for sub-components of the simscape model are defined below.

Springs The 4 springs supporting the suspended optical table are modelled with "bushing joints" having stiffness and damping in the x-y-z directions:

Inertial Shaker (IS20) The inertial shaker is defined as two solid bodies:

- the "housing" that is fixed to the element that we want to excite

- the "inertial mass" that is suspended inside the housing

The inertial mass is guided inside the housing and an actuator (coil and magnet) can be used to apply a force between the inertial mass and the support. The "reacting" force on the support is then used as an excitation.

Characteristic	Value
Output Force	20 N
Frequency Range	10-3000 Hz
Moving Mass	0.1 kg
Total Mass	0.3 kg

Table 2.2: Summary of the IS20 datasheet

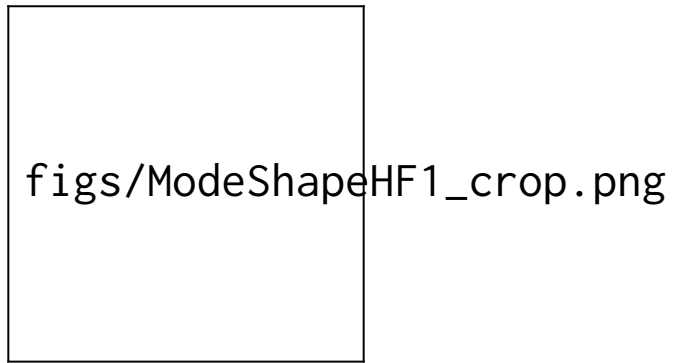**Figure 2.3:** Mode shapes of the 6 suspension modes (from 1Hz to 9Hz)

figs/ModeShapeHF1_crop.png

Figure 2.4: First flexible mode of the table at 700Hz
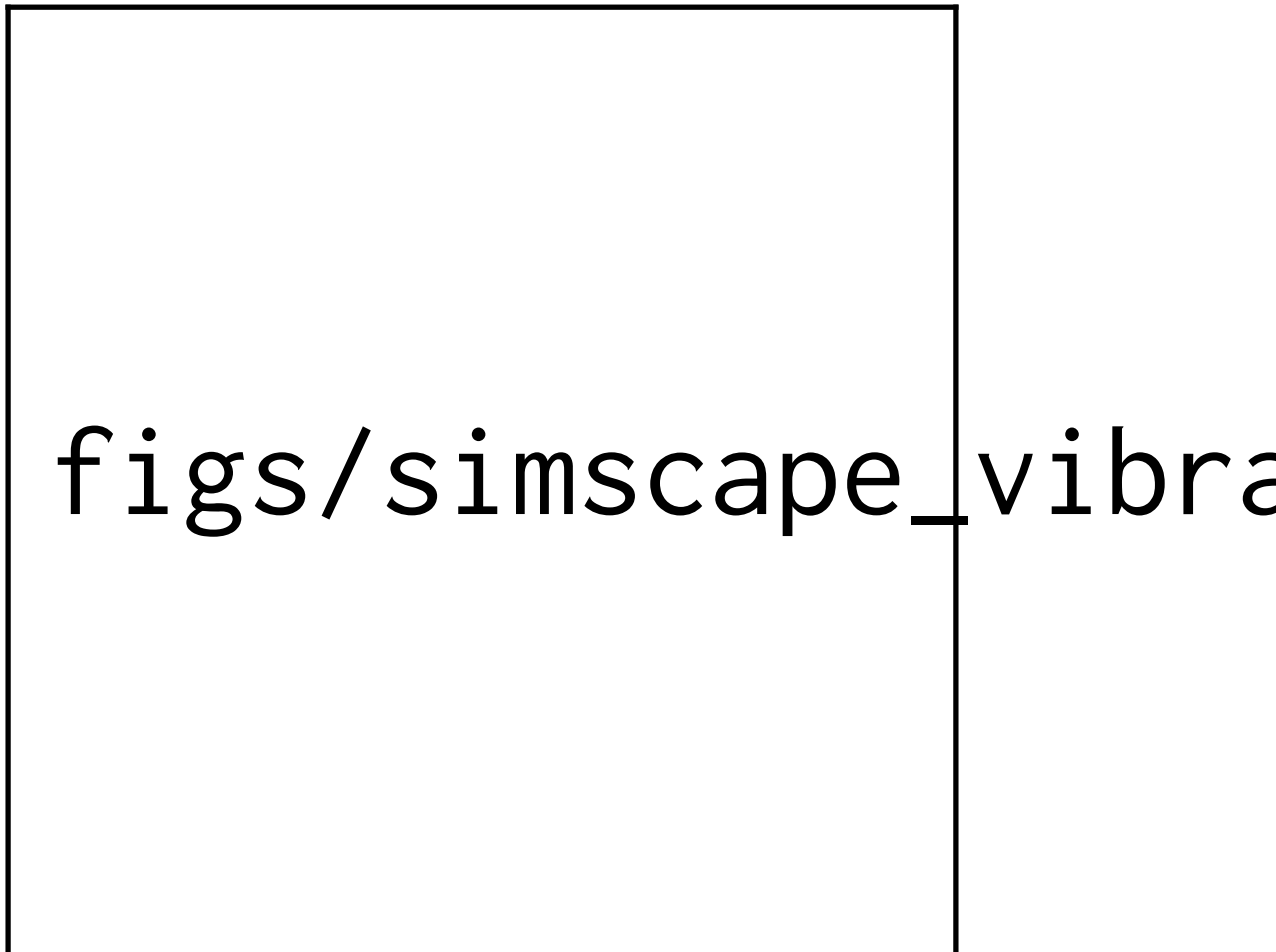
figs/simscape_vibra

Figure 2.5: 3D representation of the simscape model

From the datasheet in Table 2.2, we can estimate the parameters of the physical shaker.

These parameters are defined below

3D accelerometer (356B18) An accelerometer consists of 2 solids:

- a "housing" rigidly fixed to the measured body

- an "inertial mass" suspended inside the housing by springs and guided in the measured direction

The relative motion between the housing and the inertial mass gives a measurement of the acceleration of the measured body (up to the suspension mode of the inertial mass).

Characteristic	Value
Sensitivity	0.102 V/(m/s2)
Frequency Range	0.5 to 3000 Hz
Resonance Frequency	¿ 20 kHz
Resolution	0.0005 m/s2 rms
Weight	0.025 kg
Size	20.3x26.1x20.3 [mm]

Table 2.3: Summary of the 356B18 datasheet

2.4.2 Identification

Let's now identify the resonance frequency and mode shapes associated with the suspension modes of the optical table.

```
──────────────────────────── Results ────────────────────────────
size(G)
State-space model with 6 outputs, 6 inputs, and 12 states.
```

Compute the resonance frequencies

	x	y	Rz	Dz	Rx	Ry
Simscape	1.28	1.28	1.82	6.78	9.47	9.47
Experimental	1.3	1.3	1.95	6.85	8.9	9.5

And the associated response of the optical table The results are shown in Table 2.4. The motion associated to the mode shapes are just indicative.

ω_0 [Hz]	8.2	8.2	8.2	5.8	5.6	5.6
x	0.0	0.0	0.0	0.0	0.1	0.5
y	0.0	0.0	0.0	0.0	0.5	0.0
z	0.0	0.0	0.0	1.0	0.0	0.0
Rx	1.0	0.0	0.0	0.0	0.8	0.0
Ry	0.0	1.0	0.0	0.0	0.2	0.9
Rz	0.0	0.0	1.0	0.0	0.0	0.0

Table 2.4: Resonance frequency and approximation of the mode shapes

3 Nano-Hexapod Dynamics

In Figure 3.1 is shown a block diagram of the experimental setup. When possible, the notations are consistent with this diagram and summarized in Table 3.1.
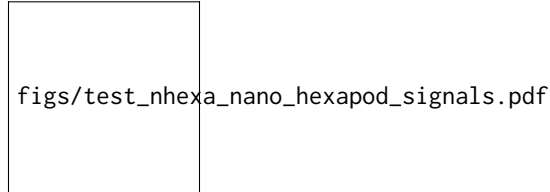

figs/test_nhexa_nano_hexapod_signals.pdf

Figure 3.1: Block diagram of the system with named signals

	Unit	Matlab	Vector	Elements
Control Input (wanted DAC voltage)	[V]	u	$\boldsymbol{u}$	u_i
DAC Output Voltage	[V]	u	$\tilde{\boldsymbol{u}}$	$\tilde{u}_i$
PD200 Output Voltage	[V]	ua	$\boldsymbol{u}_a$	$u_{a,i}$
Actuator applied force	[N]	tau	$\boldsymbol{\tau}$	τ_i
Strut motion	[m]	dL	$d\boldsymbol{\mathcal{L}}$	$d\mathcal{L}_i$
Encoder measured displacement	[m]	dLm	$d\boldsymbol{\mathcal{L}}_m$	$d\mathcal{L}_{m,i}$
Force Sensor strain	[m]	epsilon	$\boldsymbol{\epsilon}$	ϵ_i
Force Sensor Generated Voltage	[V]	taum	$\tilde{\boldsymbol{\tau}}_m$	$\tilde{\tau}_{m,i}$
Measured Generated Voltage	[V]	taum	$\boldsymbol{\tau}_m$	$\tau_{m,i}$
Motion of the top platform	[m,rad]	dX	$d\boldsymbol{\mathcal{X}}$	$d\mathcal{X}_i$
Metrology measured displacement	[m,rad]	dXm	$d\boldsymbol{\mathcal{X}}_m$	$d\mathcal{X}_{m,i}$

Table 3.1: List of signals

It is structured as follow:

- Section 3.1: The dynamics of the nano-hexapod is identified.

- Section 4.1: The identified dynamics is compared with the Simscape model.

3.1 Identification of the dynamics

In this section, the dynamics of the nano-hexapod with the encoders fixed to the plates is identified.

First, the measurement data are loaded in Section 3.1.1, then the transfer function matrix from the actuators to the encoders are estimated in Section 3.1.2. Finally, the transfer function matrix from the actuators to the force sensors is estimated in Section 3.1.3.
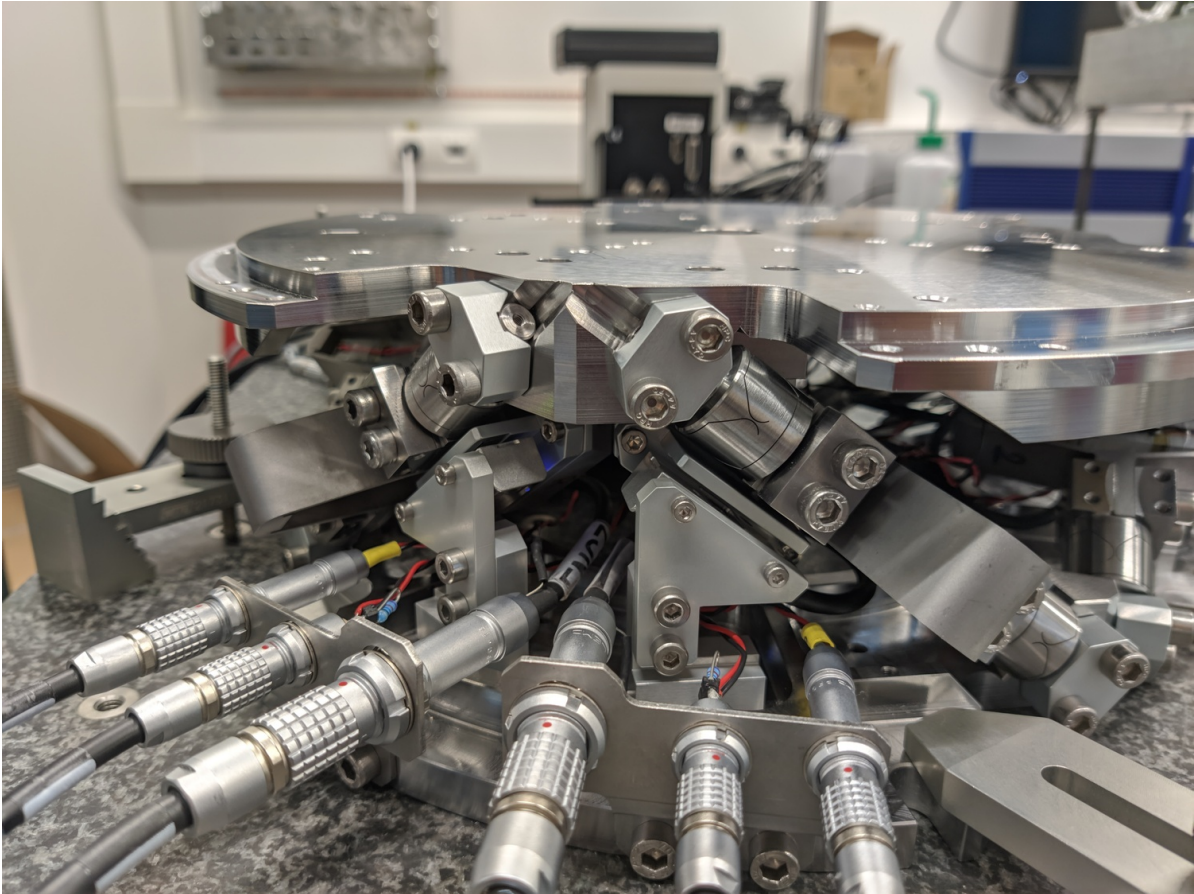
Figure 3.2: Nano-Hexapod with encoders fixed to the struts

3.1.1 Data Loading and Spectral Analysis Setup

The actuators are excited one by one using a low pass filtered white noise. For each excitation, the 6 force sensors and 6 encoders are measured and saved.

3.1.2 Transfer function from Actuator to Encoder

The 6x6 transfer function matrix from the excitation voltage u and the displacement $d\mathcal{L}_m$ as measured by the encoders is estimated.

The diagonal and off-diagonal terms of this transfer function matrix are shown in Figure 3.3.
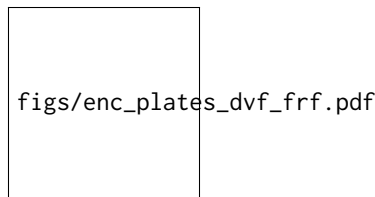

figs/enc_plates_dvf_frf.pdf

Figure 3.3: Measured FRF for the transfer function from u to $d\mathcal{L}_m$

> **Important**
>
> From Figure 3.3, we can draw few conclusions on the transfer functions from u to $d\mathcal{L}_m$ when the encoders are fixed to the plates:
>
> - the decoupling is rather good at low frequency (below the first suspension mode). The low frequency gain is constant for the off diagonal terms, whereas when the encoders where fixed to the struts, the low frequency gain of the off-diagonal terms were going to zero (Figure **??**).
>
> - the flexible modes of the struts at 226Hz and 337Hz are indeed shown in the transfer functions, but their amplitudes are rather low.
>
> - the diagonal terms have alternating poles and zeros up to at least 600Hz: the flexible modes of the struts are not affecting the alternating pole/zero pattern. This what not the case when the encoders were fixed to the struts (Figure **??**).

3.1.3 Transfer function from Actuator to Force Sensor

Then the 6x6 transfer function matrix from the excitation voltage u and the voltage τ_m generated by the Force senors is estimated. The bode plot of the diagonal and off-diagonal terms are shown in Figure 3.4.

> **Important**
>
> It is shown in Figure 4.2 that:
>
> - The IFF plant has alternating poles and zeros

Figure 3.4: Measured FRF for the IFF plant

- The first flexible mode of the struts as 235Hz is appearing, and therefore is should be possible to add some damping to this mode using IFF

- The decoupling is quite good at low frequency (below the first model) as well as high frequency (above the last suspension mode, except near the flexible modes of the top plate)

3.1.4 Save Identified Plants

The identified dynamics is saved for further use.

3.2 Effect of Payload mass on the Dynamics

In this section, the encoders are fixed to the plates, and we identify the dynamics for several payloads. The added payload are half cylinders, and three layers can be added for a total of around 40kg (Figure 3.5).

First the dynamics from $\boldsymbol{u}$ to $d\boldsymbol{\mathcal{L}}_m$ and $\boldsymbol{\tau}_m$ is identified. Then, the Integral Force Feedback controller is developed and applied as shown in Figure 3.6. Finally, the dynamics from $\boldsymbol{u}'$ to $d\boldsymbol{\mathcal{L}}_m$ is identified and the added damping can be estimated.

3.2.1 Measured Frequency Response Functions

The following data are loaded:

- `Va`: the excitation voltage (corresponding to u_i)

- `Vs`: the generated voltage by the 6 force sensors (corresponding to $\boldsymbol{\tau}_m$)

- `de`: the measured motion by the 6 encoders (corresponding to $d\boldsymbol{\mathcal{L}}_m$)

The window `win` and the frequency vector `f` are defined. Finally the 6×6 transfer function matrices from $\boldsymbol{u}$ to $d\boldsymbol{\mathcal{L}}_m$ and from $\boldsymbol{u}$ to $\boldsymbol{\tau}_m$ are identified: The identified dynamics are then saved for further use.
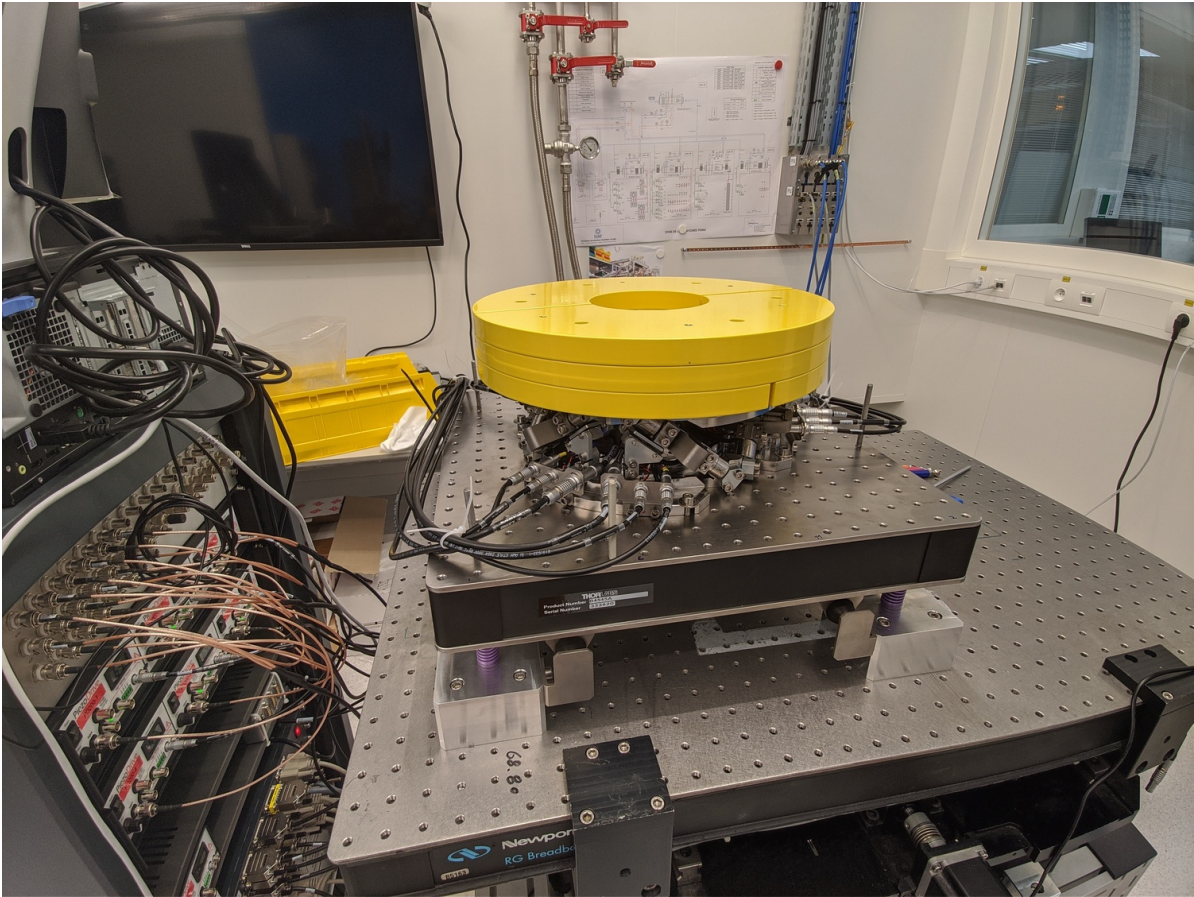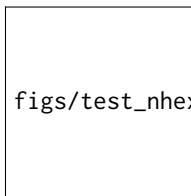
Figure 3.5: Picture of the nano-hexapod with added mass

figs/test_nhexa_nano_hexapod_signals_iff.pdf

Figure 3.6: Block Diagram of the experimental setup and model

3.2.2 Transfer function from Actuators to Encoders

The transfer functions from $\boldsymbol{u}$ to $d\boldsymbol{\mathcal{L}}_m$ are shown in Figure 3.7.
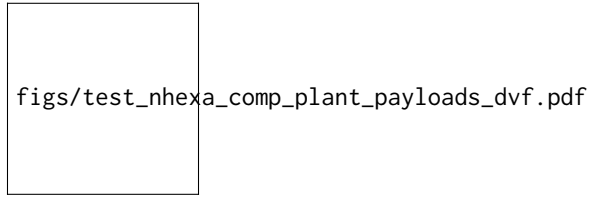

Figure 3.7: Measured Frequency Response Functions from u_i to $d\mathcal{L}_{m,i}$ for all 4 payload conditions. Diagonal terms are solid lines, and shaded lines are off-diagonal terms.

> **Important**
>
> From Figure 3.7, we can observe few things:
>
> - The obtained dynamics is changing a lot between the case without mass and when there is at least one added mass.
>
> - Between 1, 2 and 3 added masses, the dynamics is not much different, and it would be easier to design a controller only for these cases.
>
> - The flexible modes of the top plate is first decreased a lot when the first mass is added (from 700Hz to 400Hz). This is due to the fact that the added mass is composed of two half cylinders which are not fixed together. Therefore is adds a lot of mass to the top plate without adding a lot of rigidity in one direction. When more than 1 mass layer is added, the half cylinders are added with some angles such that rigidity are added in all directions (see Figure 3.5). In that case, the frequency of these flexible modes are increased. In practice, the payload should be one solid body, and we should not see a massive decrease of the frequency of this flexible mode.
>
> - Flexible modes of the top plate are becoming less problematic as masses are added.
>
> - First flexible mode of the strut at 230Hz is not much decreased when mass is added. However, its apparent amplitude is much decreased.

3.2.3 Transfer function from Actuators to Force Sensors

The transfer functions from $\boldsymbol{u}$ to $\boldsymbol{\tau}_m$ are shown in Figure 3.8.
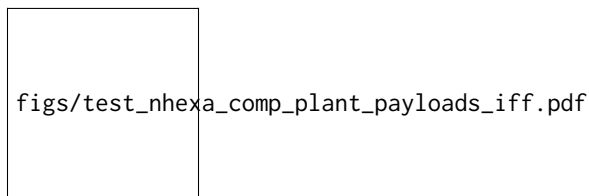

Figure 3.8: Measured Frequency Response Functions from u_i to $\tau_{m,i}$ for all 4 payload conditions. Diagonal terms are solid lines, and shaded lines are off-diagonal terms.

> **Important**
>
> From Figure 3.8, we can see that for all added payloads, the transfer function from $\boldsymbol{u}$ to $\boldsymbol{\tau}_m$ always has alternating poles and zeros.

3.2.4 Coupling of the transfer function from Actuator to Encoders

The RGA-number, which is a measure of the interaction in the system, is computed for the transfer function matrix from $\boldsymbol{u}$ to $d\boldsymbol{\mathcal{L}}_m$ for all the payloads. The obtained numbers are compared in Figure 3.9.
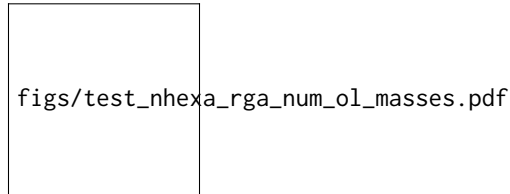
Figure 3.9: RGA-number for the open-loop transfer function from $\boldsymbol{u}$ to $d\boldsymbol{\mathcal{L}}_m$

> **Important**
>
> From Figure 3.9, it is clear that the coupling is quite large starting from the first suspension mode of the nano-hexapod. Therefore, is the payload's mass is increase, the coupling in the system start to become unacceptably large at lower frequencies.

3.3 Conclusion

> **Important**
>
> In this section, the dynamics of the nano-hexapod with the encoders fixed to the plates is studied. It has been found that:
>
> - The measured dynamics is in agreement with the dynamics of the simscape model, up to the flexible modes of the top plate. See figures 4.3 and 4.4 for the transfer function to the force sensors and Figures 4.6 and 4.7 for the transfer functions to the encoders
>
> - The Integral Force Feedback strategy is very effective in damping the suspension modes of the nano-hexapod (Figure **??**).
>
> - The transfer function from $\boldsymbol{u}'$ to $d\boldsymbol{\mathcal{L}}_m$ show nice dynamical properties and is a much better candidate for the high-authority-control than when the encoders were fixed to the struts. At least up to the flexible modes of the top plate, the diagonal elements of the transfer function matrix have alternating poles and zeros, and the phase is moving smoothly. Only the flexible modes of the top plates seems to be problematic for control.

4 Comparison with the Nano-Hexapod model?

4.1 Comparison with the Simscape Model

In this section, the measured dynamics done in Section 3.1 is compared with the dynamics estimated from the Simscape model.

A configuration is added to be able to put the nano-hexapod on top of the vibration table as shown in Figure 4.1.
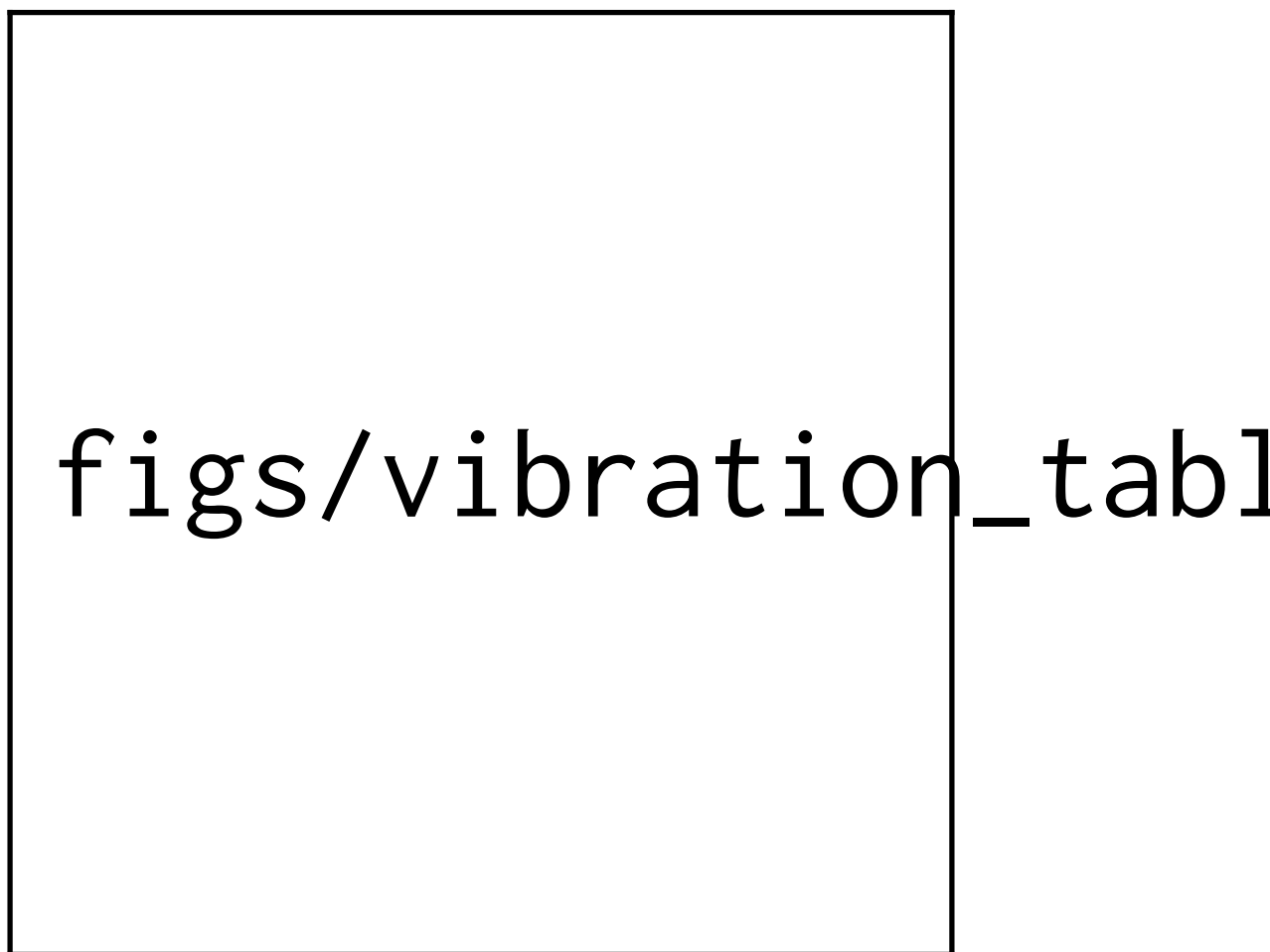

Figure 4.1: 3D representation of the simscape model with the nano-hexapod

4.1.1 Identification with the Simscape Model

The nano-hexapod is initialized with the APA taken as 2dof models. Now, the dynamics from the DAC voltage $\boldsymbol{u}$ to the encoders $d\boldsymbol{\mathcal{L}}_m$ is estimated using the Simscape model. Then the transfer function from $\boldsymbol{u}$ to $\boldsymbol{\tau}_m$ is identified using the Simscape model. The identified dynamics is saved for further use.

4.1.2 Dynamics from Actuator to Force Sensors

The identified dynamics is compared with the measured FRF:

- Figure 4.2: the individual transfer function from u_1 (the DAC voltage for the first actuator) to the force sensors of all 6 struts are compared

- Figure 4.3: all the diagonal elements are compared

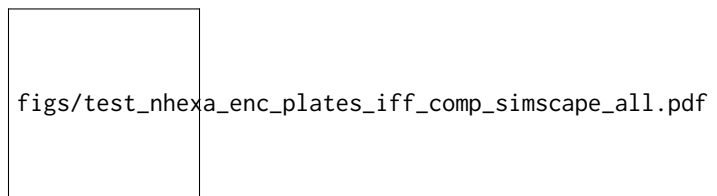- Figure 4.4: all the off-diagonal elements are compared

figs/test_nhexa_enc_plates_iff_comp_simscape_all.pdf

Figure 4.2: IFF Plant for the first actuator input and all the force senosrs

figs/test_nhexa_enc_plates_iff_comp_simscape.pdf
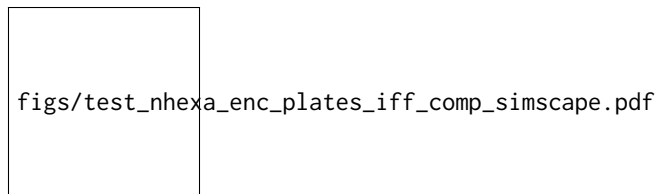
Figure 4.3: Diagonal elements of the IFF Plant

figs/test_nhexa_enc_plates_iff_comp_offdiag_simscape.pdf
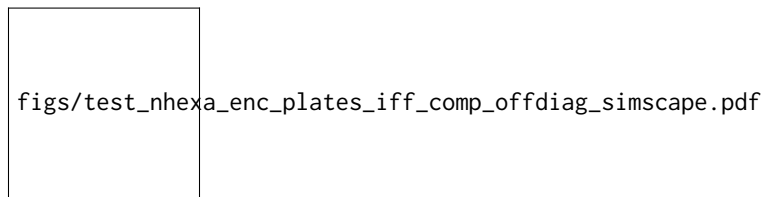
Figure 4.4: Off diagonal elements of the IFF Plant

4.1.3 Dynamics from Actuator to Encoder

The identified dynamics is compared with the measured FRF:

- Figure 4.5: the individual transfer function from u_3 (the DAC voltage for the actuator number 3) to the six encoders

- Figure 4.6: all the diagonal elements are compared

- Figure 4.7: all the off-diagonal elements are compared

figs/test_nhexa_enc_plates_dvf_comp_simscape_all.pdf

Figure 4.5: DVF Plant for the first actuator input and all the encoders

figs/test_nhexa_enc_plates_dvf_comp_simscape.pdf
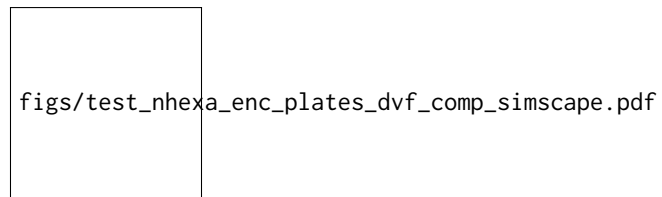
Figure 4.6: Diagonal elements of the DVF Plant

figs/test_nhexa_enc_plates_dvf_comp_offdiag_simscape.pdf
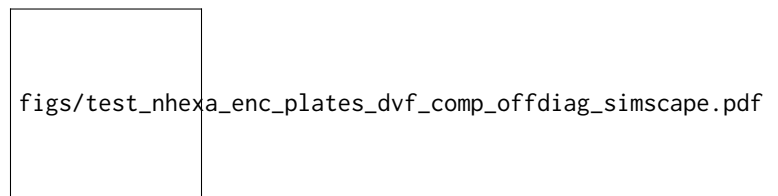
Figure 4.7: Off diagonal elements of the DVF Plant

4.1.4 Conclusion

> **Important**
>
> The Simscape model is quite accurate for the transfer function matrices from $\boldsymbol{u}$ to $\boldsymbol{\tau}_m$ and from $\boldsymbol{u}$ to $d\boldsymbol{\mathcal{L}}_m$ except at frequencies of the flexible modes of the top-plate. The Simscape model can therefore be used to develop the control strategies.

4.2 Comparison with the Simscape model

Let's now compare the identified dynamics with the Simscape model. We wish to verify if the Simscape model is still accurate for all the tested payloads.

4.2.1 System Identification

Let's initialize the simscape model with the nano-hexapod fixed on top of the vibration table. First perform the identification for the transfer functions from $\boldsymbol{u}$ to $d\boldsymbol{\mathcal{L}}_m$: The identified dynamics are then saved for further use.

4.2.2 Transfer function from Actuators to Encoders

The measured FRF and the identified dynamics from u_i to $d\mathcal{L}_{m,i}$ are compared in Figure 4.8. A zoom near the "suspension" modes is shown in Figure 4.9.
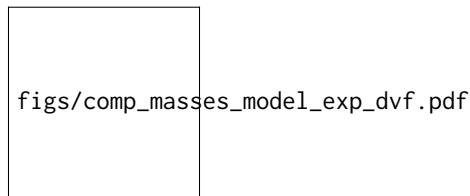
figs/comp_masses_model_exp_dvf.pdf

Figure 4.8: Comparison of the transfer functions from u_i to $d\mathcal{L}_{m,i}$ - measured FRF and identification from the Simscape model

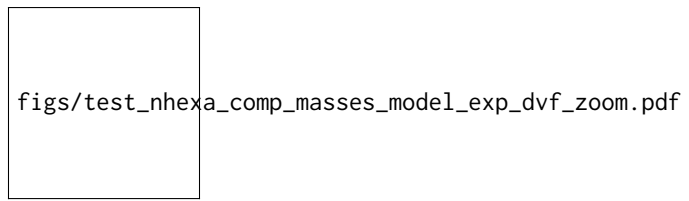figs/test_nhexa_comp_masses_model_exp_dvf_zoom.pdf

Figure 4.9: Comparison of the transfer functions from u_i to $d\mathcal{L}_{m,i}$ - measured FRF and identification from the Simscape model (Zoom)

> **Important**
>
> The Simscape model is very accurately representing the measured dynamics up. Only the flexible modes of the struts and of the top plate are not represented here as these elements are modelled as rigid bodies.

4.2.3 Transfer function from Actuators to Force Sensors

The measured FRF and the identified dynamics from u_i to $\tau_{m,i}$ are compared in Figure 4.10. A zoom near the "suspension" modes is shown in Figure 4.11.
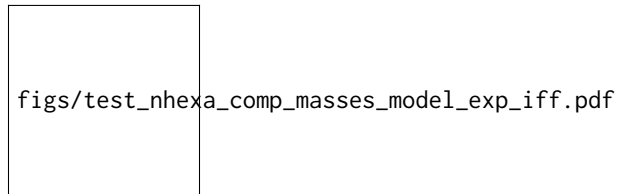
Figure 4.10: Comparison of the transfer functions from u_i to $\tau_{m,i}$ - measured FRF and identification from the Simscape model
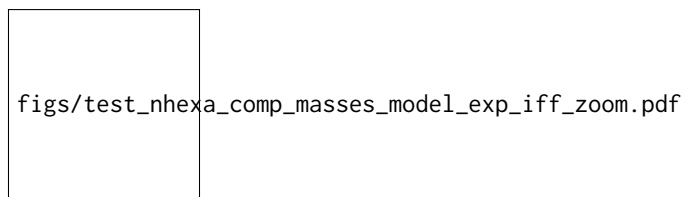

Figure 4.11: Comparison of the transfer functions from u_i to $\tau_{m,i}$ - measured FRF and identification from the Simscape model (Zoom)

Bibliography

[1] S. Skogestad and I. Postlethwaite, *Multivariable Feedback Control: Analysis and Design - Second Edition*. John Wiley, 2007.

[2] M. Indri and R. Oboe, *Mechatronics and Robotics: New Trends and Challenges*. CRC Press, 2020.